Epitaxial fabrication of two-dimensional $NiSe_2$ on Ni(111) substrate

Yan Shao, Shiru Song, Xu Wu, Jing Qi, Hongliang Lu, Chen Liu, Shiyu Zhu, Zhongliu Liu, Jiaou Wang, Dongxia Shi, Shixuan Du, Yeliang Wang, and H.-J. Gao

Citation: Appl. Phys. Lett. **111**, 113107 (2017);
View online: https://doi.org/10.1063/1.4991065
View Table of Contents: http://aip.scitation.org/toc/apl/111/11
Published by the American Institute of Physics

Epitaxial fabrication of two-dimensional $NiSe_2$ on Ni(111) substrate

Yan Shao,[1,2,a)] Shiru Song,[1,2,a)] Xu Wu,[1,2] Jing Qi,[1,2] Hongliang Lu,[1,2] Chen Liu,[3] Shiyu Zhu,[1,2] Zhongliu Liu,[1,2] Jiaou Wang,[3] Dongxia Shi,[1,2] Shixuan Du,[1,2,4,b)] Yeliang Wang,[1,2,4,b)] and H.-J. Gao[1,2,4]

[1]*Institute of Physics and University of Chinese Academy of Sciences, Chinese Academy of Sciences, Beijing 100190, China*
[2]*Beijing Key Laboratory for Nanomaterials and Nanodevices, Beijing 100190, China*
[3]*Institute of High Energy Physics, Chinese Academy of Sciences, Beijing 100049, China*
[4]*Collaborative Innovation Center of Quantum Matter, Beijing 100084, China*

(Received 20 June 2017; accepted 4 September 2017; published online 15 September 2017)

Two-dimensional (2D) transition metal dichalcogenides (TMDs) receive significant attention due to their intriguing physical properties for both fundamental research and potential applications in electronics, optoelectronics, and catalysis. A high-quality 2D film of $NiSe_2$, a TMD material, is grown epitaxially by a single step direct selenization of a Ni(111) substrate. X-ray photoemission spectroscopy, low-energy electron diffraction, scanning tunneling microscopy, and density functional theory calculations are combined to confirm the formation and structure of the film, revealing a $(\sqrt{3} \times \sqrt{3})$ superlattice of the $NiSe_2$ film formed on the $(\sqrt{7} \times \sqrt{7})$ superlattice of the substrate. Fabrication of this 2D $NiSe_2$ film opens opportunities to research its applications, especially for electrocatalysis and energy storage devices. *Published by AIP Publishing.*
[http://dx.doi.org/10.1063/1.4991065]

Discovery of exotic properties in graphene has reinvigorated interest in other two-dimensional (2D) layered materials.[1–7] In particular, 2D transition metal dichalcogenides (TMDs) with the generalized formula MX_2, where M represents a transition metal from groups 4–12 and X is a chalcogen (S, Se, or Te), have received significant attention in the last few years.[8–11] This enthusiasm is due mainly to the various valuable properties of bulk TMDs—e.g., having a special electronic character (ranging from insulator or semiconductor to semimetal or true metal,[12] being superconductive[13,14] or catalytic,[15,16] supporting charge density wave formation,[14] or having another uncommon optical or thermal property[12,17]—any of which would generally be preserved in a 2D counterpart. Moreover, interesting characteristics may be found in 2D TMDs that were unnoticed or nonexistent in their bulk counterparts due to spin-orbit coupling or quantum confinement effects.[18–23] For example, when monolayer MoS_2 is cut away from the bulk, it shows an indirect-to-direct bandgap transition, making it a promising material for electronic and optoelectronic applications.[24–26] Many other 2D TMD materials with outstanding properties and promising applications have also become hot topics of research in recent years.[27–31]

Among these, 2D NiX_2 (X = S and Se) is a rarely studied group of TMD materials, even though the 3D counterparts are known to have many intriguing properties and applications, especially in electrocatalysis and energy storage devices.[15,32–37] Bulk $NiSe_2$, for example, is a Pauli paramagnetic metal with high electrical conductivity. Its high reversible capacity and good cycle ability as an electrode have been demonstrated, making it a promising cathode material for rechargeable lithium batteries.[33] Moreover, $NiSe_2$ nanoparticles and nanosheets exhibit superior electrocatalytic and photocatalytic efficiency in such like oxygen evolution reactions (OER) and hydrogen evolution reactions (HER) in very recent studies.[34–36] Considering the high cost and scarcity of Pt-based catalysts, the low cost, earth-abundant Ni-based material $NiSe_2$ has shown promise for practical water-splitting solar cells. Two-dimensional TMD nanomaterials are generally believed to have advantages over their bulk phase, both in electrocatalysis and as electrodes, benefiting from their high surface-to-volume ratio. Some quasi-2D $NiSe_2$ materials such as $NiSe_2$ nanosheets have been produced.[35,36] However, the research on 2D layered $NiSe_2$ published so far consists only of theoretical calculations,[38,39] and experimentally fabricated 2D $NiSe_2$ films are urgently needed.

In this letter, we report epitaxial growth of 2D, layered $NiSe_2$ on a Ni(111) substrate by direct selenization. We utilized single-crystal Ni(111) bi-functionally, as both the Ni source and the substrate. Pure Se particles were first filled into the ceramic Knudsen cell. Before the deposition, the Se source was degassed for more than 20 h at 100 °C and then heated up to 130 °C for 2 h to keep the flux stable. After a deposition of 20 min, the as-deposited sample was annealed to 320 °C for 30 min, until a well-ordered structure was observed by low-energy electron diffraction (LEED). The whole fabrication process was monitored *in-situ* by X-ray photoemission spectroscopy (XPS). The atomic structure of the epitaxial $NiSe_2$ film was determined by a combination of low-energy electron diffraction (LEED) and scanning tunneling microscopy (STM). We then performed density functional theory (DFT) calculations to better elucidate this structure. Our experimental observations combined with the calculated results support the conclusion that we fabricated high-quality 2D $NiSe_2$ films on the Ni(111) substrate, which may have promising applications in electrocatalysis and energy storage devices.[35,36]

[a)]Y. Shao and S. Song contributed equally to this work.
[b)]Electronic addresses: sxdu@iphy.ac.cn and ylwang@iphy.ac.cn

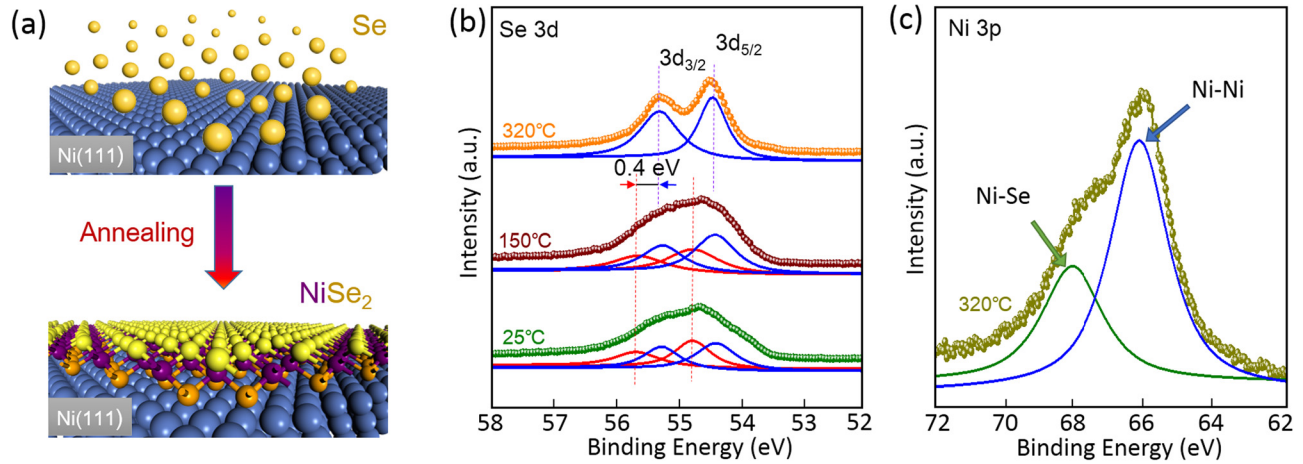

FIG. 1. Growth process and XPS spectra of the $NiSe_2$ film. (a) Schematic of the fabrication process of $NiSe_2$ thin films by direct selenization of the Ni(111) substrate. Top-layer Se, middle-layer Ni, and bottom-layer Se atoms in sandwiched $NiSe_2$ are shown in yellow, purple, and orange, respectively. (b) XPS measurements for the binding energies of Se 3d electrons during $NiSe_2$ growth, revealing the change in the chemical state of Se from Se^0 (colored in red) to Se^{-2} (colored in blue) and the full crystallization and complete formation of $NiSe_2$ films at 320 °C. (c) XPS measurements for the binding energies of the Ni 3p electron after $NiSe_2$ growth, demonstrating two states of Ni atoms—the Ni-Ni state in Ni substrate (colored in blue) and the Ni-Se state in $NiSe_2$ films (colored in green).

Our experiments were performed in an ultrahigh vacuum (UHV) system with a base pressure of about 2×10^{-10} mbar. The Ni(111) substrate was cleaned by several cycles of sputtering and annealing until it yielded a distinct Ni (1×1) diffraction spot in a LEED pattern and clean surface terraces in STM images. The fabrication process is shown schematically in Fig. 1(a): selenium atoms were deposited onto a cleaned Ni(111) surface, and then the as-deposited sample was annealed at 320 °C for 30 min to obtain epitaxial $NiSe_2$ films. The chamber pressure is in the range of (5–8) $\times 10^{-10}$ mbar during the UHV annealing and the selenization process. The growth process of $NiSe_2$ thin films was monitored *in situ* by X-ray photoemission spectroscopy (XPS).

Figure 1(b) shows the characteristic XPS spectra from the core level of Se 3d before and during annealing. After Se atoms were deposited on the Ni(111) surface at room temperature (RT), the XPS spectra (colored in green) were revealed in two pairs of peaks. The two red peaks are located at binding energies of 55.70 and 54.76 eV, respectively, corresponding to the characteristic signals of Se^0 $3d_{3/2}$ and $3d_{5/2}$ peaks. The other two blue peaks appear at binding energies of 55.24 and 54.35 eV, corresponding to the characteristic signals of Se^{-2} $3d_{3/2}$ and $3d_{5/2}$ peaks. The shift between the two pairs of peaks is about 0.4–0.5 eV, which can be explained by a change in the chemical state of Se from Se^0 to Se^{-2}, demonstrating the selenization process of the sample.[27] As the sample was annealed to about 150 °C, the XPS spectra (colored in purple) show a decreasing intensity of Se^0 peaks and an increasing intensity of Se^{2-} peaks. After the annealing process at 320 °C, the Se^0 peaks disappear and the XPS spectra (colored in orange) show only two blue peaks (at 55.30 and 54.42 eV), representing Se^{-2} $3d_{3/2}$ and $3d_{5/2}$ peaks, indicating full crystallization and complete formation of $NiSe_2$ films. It also suggests that excessive Se atoms desorbed from the substrate and no additional Se atoms left on the substrate. The XPS spectra of Ni 3p electrons after the growth of $NiSe_2$ film are shown in Fig. 1(c), which includes two peaks, clearly demonstrating two states of Ni atoms—the Ni-Ni state in the Ni substrate (colored in blue) and the Ni-Se state in the $NiSe_2$ film (colored in green).

The structural order of the $NiSe_2$ films on the Ni(111) surface can be characterized macroscopically by LEED, as shown in Fig. 2(a). The outer six bright spots, circled by the blue dashed line, can be easily assigned to the Ni(111) substrate with six-fold symmetry. The other distinct diffraction spots originate from the $NiSe_2$ superstructure. To identify the

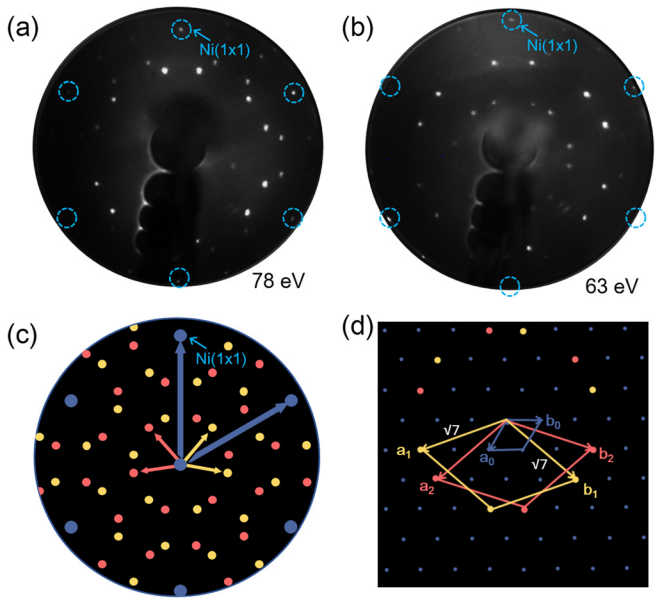

FIG. 2. LEED patterns and corresponding schematics of $NiSe_2$ superstructure formed on Ni(111). (a) LEED pattern obtained with the incident electron beam energy of 78 eV. The outer six bright spots highlighted by the blue dashed circles originate from the six-fold symmetry of the Ni(111) substrate. The additional diffraction spots are ascribed to the $NiSe_2$ film. (b) LEED pattern obtained with a lower incident electron beam energy of 63 eV; more diffraction spots from the $NiSe_2$ film are visible. (c) Sketch of the diffraction spots shown in (a) and (b), where the reciprocal vectors of each group of spots are indicated by blue, red, and yellow arrows, respectively. (d) Schematic diagram of the diffraction spots in real space. These data reveal a $(\sqrt{7} \times \sqrt{7})$ superstructure of the $NiSe_2$ film [lattice vectors ($\mathbf{a_1}$, $\mathbf{b_1}$) or ($\mathbf{a_2}$, $\mathbf{b_2}$)] with respect to the Ni(111) lattice [lattice vectors ($\mathbf{a_0}$, $\mathbf{b_0}$)].

superstructure in this LEED pattern better, we lowered the incident electron beam energy, which led to clearer imaging of the inner diffraction spots, as shown in Fig. 2(b). For clarity, we sketched a map of the diffraction spots of the superstructure in reciprocal space [Fig. 2(c)], where the reciprocal vectors of each group of spots are indicated by different colored arrows. Besides the (1×1) diffraction spots from the Ni(111) lattice, two symmetrically equivalent domains exist, identified by red and yellow spots, respectively. For a more thorough understanding of this LEED pattern, a schematic diagram in real space consistent with the diffraction patterns is provided in Fig. 2(d). This diagram directly reveals the commensurate relation between the $NiSe_2$ adlayer and the substrate lattice. The matrix of this superstructure is $\begin{bmatrix} 1 & -2 \\ 2 & 3 \end{bmatrix}$ or the equivalent $\begin{bmatrix} 2 & -1 \\ 1 & 3 \end{bmatrix}$, and the corresponding angles between the close-packed direction Ni[1 − 10] and the superstructure can be obtained as 40.9° and 19.1°, respectively. From these data, the $NiSe_2$ adlayer can be easily identified as a $(\sqrt{7} \times \sqrt{7})$ superstructure with respect to the Ni(111) substrate. Furthermore, identical LEED patterns were observed on the entire sample surface (4 mm × 4 mm in size), indicating the growth of a homogeneous and high-quality film.

To investigate the atomic structure of the $NiSe_2$ film in real space, we performed STM studies. A large-scale STM image is shown in the inset of Fig. 3(a), which demonstrates the high quality of the $NiSe_2$ film. Figure 3(a) is a medium-scale STM image of the area delineated by the white square in the large-scale STM image, revealing a well-ordered moiré pattern of the $NiSe_2$ thin film on Ni(111). In order to better investigate the structure of the moiré pattern, we zoomed in the scanning area and obtained a higher-resolution STM image, as shown in Fig. 3(b). One of the supercells is marked by the black rhombus. The orientation of this superstructure has a rotation about 41° with respect to the Ni[1 − 10] direction. The periodicity of this moiré pattern is about 6.59 Å [Fig. 3(d)], as measured by the profile line along the orientation of this superstructure [corresponding to the purple dashed line in Fig. 3(b)]. The periodicity is equal to the dimension of the $(\sqrt{7} \times \sqrt{7})$ superlattice of the Ni(111) substrate [the surface lattice constant of Ni(111) is 2.492 Å, $\sqrt{7} \times 2.492$ Å = 6.593 Å]. It is apparent that both the orientations and the periodicity of the $NiSe_2$ superstructure detected by STM are in good agreement with our LEED analysis, confirming that a $(\sqrt{7} \times \sqrt{7})$ superstructure formed on the Ni(111) surface. Thus, our STM observations confirm a continuous grain over 100 nm × 100 nm and the LEED patterns suggest a homogeneous and high-quality film.

Figure 3(c) shows an atomic-resolution STM image of the area indicated by the white square in Fig. 3(b), revealing hexagonally arranged bright protrusions. The unit cell of the $(\sqrt{7} \times \sqrt{7})$ superstructure is marked by a black rhombus. The distance between the nearest two protrusions can be measured by the blue dashed line profile, as shown in Fig. 3(e), showing that the distance is about 3.80 Å, which agrees quite well with the lattice constant of 1T-$NiSe_2$ structure mentioned in an earlier calculation report.[38] Note that STM images only the topmost layer atoms of X-M-X layered TMD materials.[27,40] Therefore, we interpret the hexagonal protrusions in Fig. 3(b) to be the Se atoms in the topmost Se plane of a $NiSe_2$ film. The tiny differences in brightness of the protrusions can be ascribed to the different relative positions between the topmost Se atoms and the Ni(111) substrate. Moreover, the moiré superstructure (the black rhombus) can be also regarded as a $(\sqrt{3} \times \sqrt{3})$ superlattice with respect to the $NiSe_2$ lattice (the lattice constant of $NiSe_2$ is 3.80 Å, $\sqrt{3} \times 3.80$ Å = 6.58 Å) with a rotation of 30°. Therefore, based on the LEED and STM measurements, a complete structural model can be established with the $(\sqrt{3} \times \sqrt{3})$ superlattice of

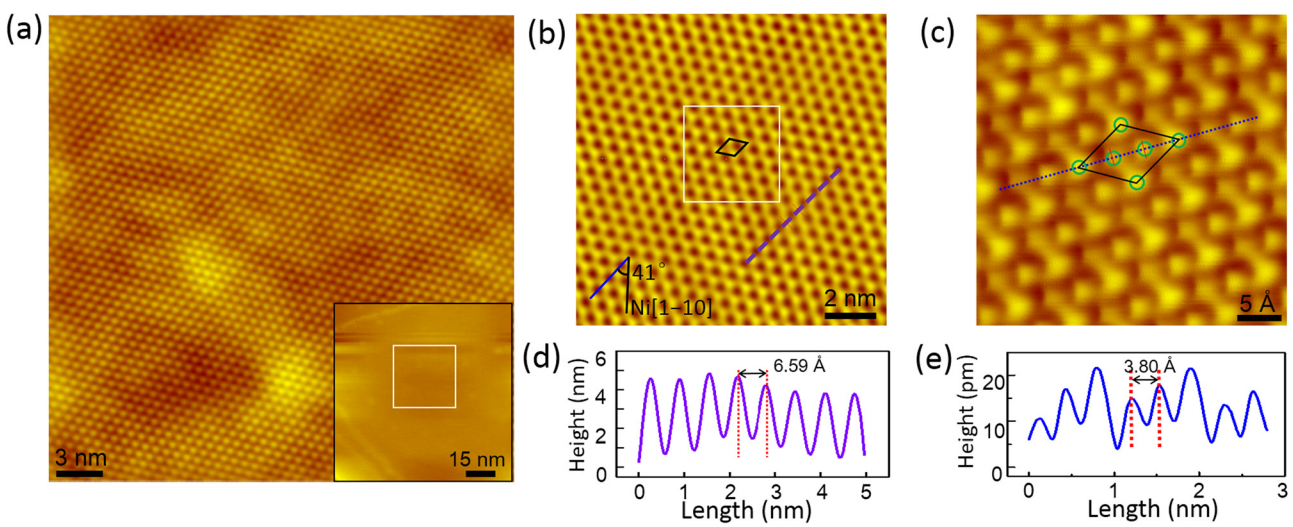

FIG. 3. STM images of the 2D $NiSe_2$ film formed on the Ni(111) surface. (a) A medium-scale STM image (−1.5 V, 0.1 nA) delineated by the white square in the large-scale STM image (the inset), presenting a well-ordered moiré pattern of the $NiSe_2$ thin film on Ni(111). Inset: Large-scale STM image (−1.5 V, 0.1 nA) of the 2D $NiSe_2$ film, demonstrating a homogeneous and high-quality $NiSe_2$ film. (b) STM image (−1.5 V, 0.1 nA) showing a clear $(\sqrt{7} \times \sqrt{7})$ superlattice with respect to the Ni(111) substrate. The angle between this superstructure and the Ni[1 − 10] close-packed direction is about 41°. (c) Atomic-resolution STM image (−1.5 V, 0.5 nA) of the area indicated by the white square in (b). The unit cell of the $(\sqrt{7} \times \sqrt{7})$ superstructure is marked by a black rhombus. The protrusions in the unit cell, marked by green circles, represent Se atoms in the topmost Se plane of the $NiSe_2$ film. (d) Line profile corresponding to the purple dashed line in (b), showing the periodicity of the moiré pattern (6.59 Å). (e) Line profile taken along the blue line in (c), revealing a periodicity of 3.80 Å in the $NiSe_2$ lattice.

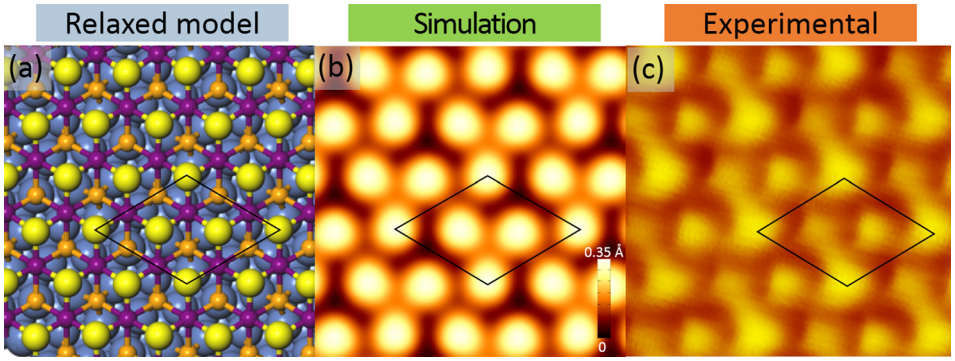

FIG. 4. Atomic configuration of the 2D $NiSe_2$ film formed on the Ni(111) surface. (a) Top view of the calculated relaxed model. In the Se-Ni-Se sandwiched structure of $NiSe_2$, the top-layer Se, middle-layer Ni, and bottom-layer Se atoms are shown in yellow, purple, and orange, respectively. (b) DFT-simulated STM image, the color scale of the apparent height is shown at the lower right corner. (c) Experimental STM image (−1.5 V, 0.5 nA); the overall features are well reproduced in (b) and the Se atoms in the top-layer are imaged. The unit cell of the moiré superstructure is marked by a black rhombus.

the $NiSe_2$ film formed on the $(\sqrt{7} \times \sqrt{7})$ superstructure of the Ni(111) substrate. A similar film, sandwiched Se-Pt-Se, has been produced by deposition of Se atoms and selenization of the Pt(111) substrate.[27]

To deeply elucidate the experimental results above, we carried out first-principles theoretical calculations within the local density approximation (LDA) by using the Vienna *ab initio* simulation package (VASP).[41,42] The projector augmented wave method was employed.[42,43] The periodic slab models included four layers of the Ni substrate, one layer $NiSe_2$, and a vacuum layer of 15 Å. All atoms were fully relaxed except for the bottom two substrate layers until the net force on every atom was less than 0.01 eV/Å. The energy cutoff of the plane-wave basis sets was 300 eV, and the k-point sampling was $11 \times 11 \times 1$ with the Monkhorst–Pack scheme. Several models of 1T-$NiSe_2$ on Ni(111), with the Ni atoms of the $NiSe_2$ film located at the atop, fcc, and hcp sites of the substrate lattice, were calculated. After these models were fully relaxed, the most stable structure with the lowest binding energy was adopted and is shown in Fig. 4(a), where top-layer Se, middle-layer Ni, and bottom-layer Se atoms are shown in yellow, purple, and orange, respectively. Based on this optimal relaxed model, we performed an STM simulation using the Tersoff-Hamann approach,[44,45] illustrated in Fig. 4(b), with which the overall features of the experimental STM image [Fig. 4(c)] agree well. Only the hexagonally arranged Se atoms in the topmost layer of the sandwiched $NiSe_2$ film are imaged. The remarkable agreement between the STM simulation and experimental STM observation strongly supports our conclusions and thus demonstrates the growth of a highly crystalline 2D $NiSe_2$ film on a Ni(111) substrate.

In summary, we fabricated a high-quality 2D sandwiched $NiSe_2$ film, a member of the TMD family, through single-step direct selenization of the Ni(111) substrate at a relatively low temperature (320 °C). The XPS measurement monitored the whole fabrication process. Combining LEED and STM measurements with DFT calculations, we confirmed the structure of the 1T-$NiSe_2$ film, demonstrating that a $(\sqrt{3} \times \sqrt{3})$ superlattice of the $NiSe_2$ film was formed on a $(\sqrt{7} \times \sqrt{7})$ superlattice of Ni(111) substrate. Our studies are a significant step forward in expanding the family of 2D TMD materials. Considering the low-cost and earth-abundance of Ni, further deep research should be performed, both theoretically and experimentally, to investigate the potential and promising properties and applications of such 2D $NiSe_2$ films, especially for electrocatalysis and energy storage devices. Meanwhile, exfoliation of this 2D material from the substrate is also of great importance for applications. Ultrasonication of the sample may be a feasible method to obtain $NiSe_2$ flakes, as described in our previous work on the exfoliation of the $PtSe_2$ film from the Pt substrate.[27]

Financial support of this work by the National Key R&D Projects of China (2016YFA0202300), the National Basic Research Program of China (2013CBA01600), the National Scientific Foundation of China (Nos. 51572290, 11334006, 61390501, and 51325204), and the Chinese Academy of Sciences (Nos. XDB0603 and XDB07030100) is gratefully acknowledged.

[1]K. S. Novoselov, V. I. Fal'ko, L. Colombo, P. R. Gellert, M. G. Schwab, and K. Kim, Nature **490**(7419), 192 (2012).
[2]K. S. Novoselov, A. Mishchenko, A. Carvalho, and A. H. Castro Neto, Science **353**(6298), 9439 (2016).
[3]Y. Pan, L. Zhang, L. Huang, L. Li, L. Meng, M. Gao, Q. Huan, X. Lin, Y. Wang, S. Du, H.-J. Freund, and H.-J. Gao, Small **10**(11), 2215 (2014).
[4]A. Molle, J. Goldberger, M. Houssa, Y. Xu, S. C. Zhang, and D. Akinwande, Nat. Mater. **16**(2), 163 (2017).
[5]L. Li, Y. Wang, S. Xie, X. B. Li, Y. Q. Wang, R. Wu, H. Sun, S. Zhang, and H. J. Gao, Nano Lett. **13**(10), 4671 (2013).
[6]Y. Q. Wang, X. Wu, Y. L. Wang, Y. Shao, T. Lei, J. O. Wang, S. Y. Zhu, H. Guo, L. X. Zhao, G. F. Chen, S. Nie, H. M. Weng, K. Ibrahim, X. Dai, Z. Fang, and H. J. Gao, Adv. Mater. **28**(25), 5013 (2016).
[7]X. Wu, Y. Shao, H. Liu, Z. Feng, Y. L. Wang, J. T. Sun, C. Liu, J. O. Wang, Z. L. Liu, S. Y. Zhu, Y. Q. Wang, S. X. Du, Y. G. Shi, K. Ibrahim, and H. J. Gao, Adv. Mater. **29**, 1605407 (2017).
[8]Q. H. Wang, K. Kalantar-Zadeh, A. Kis, J. N. Coleman, and M. S. Strano, Nat. Nanotechnol. **7**(11), 699 (2012).
[9]M. Chhowalla, H. S. Shin, G. Eda, L. J. Li, K. P. Loh, and H. Zhang, Nat. Chem. **5**(4), 263 (2013).
[10]C. Tan and H. Zhang, Chem. Soc. Rev. **44**(9), 2713 (2015).
[11]C. Gong, H. Zhang, W. Wang, L. Colombo, R. M. Wallace, and K. Cho, Appl. Phys. Lett. **103**(5), 053513 (2013).
[12]J. A. Wilson and A. D. Yoffe, Adv. Phys. **18**(73), 193 (1969).
[13]B. Sipos, A. F. Kusmartseva, A. Akrap, H. Berger, L. Forro, and E. Tutis, Nat. Mater. **7**(12), 960 (2008).
[14]A. H. Castro Neto, Phys. Rev. Lett. **86**(19), 4382 (2001).
[15]D. Kong, J. J. Cha, H. Wang, H. R. Lee, and Y. Cui, Energy Environ. Sci. **6**(12), 3553 (2013).
[16]A. B. Laursen, S. Kegnæs, S. Dahl, and I. Chorkendorff, Energy Environ. Sci. **5**(2), 5577 (2012).

[17]C. Muratore, V. Varshney, J. J. Gengler, J. J. Hu, J. E. Bultman, T. M. Smith, P. J. Shamberger, B. Qiu, X. Ruan, A. K. Roy, and A. A. Voevodin, Appl. Phys. Lett. **102**(8), 081604 (2013).
[18]A. Splendiani, L. Sun, Y. Zhang, T. Li, J. Kim, C. Y. Chim, G. Galli, and F. Wang, Nano Lett. **10**(4), 1271 (2010).
[19]Y. Zhang, T. R. Chang, B. Zhou, Y. T. Cui, H. Yan, Z. Liu, F. Schmitt, J. Lee, R. Moore, Y. Chen, H. Lin, H. T. Jeng, S. K. Mo, Z. Hussain, A. Bansil, and Z. X. Shen, Nat. Nanotechnol. **9**(2), 111 (2014).
[20]K. F. Mak, K. He, J. Shan, and T. F. Heinz, Nat. Nanotechnol. **7**(8), 494 (2012).
[21]K. F. Mak, C. Lee, J. Hone, J. Shan, and T. F. Heinz, Phys. Rev. Lett. **105**(13), 136805 (2010).
[22]J. A. Reyes-Retana and F. Cervantes-Sodi, Sci. Rep. **6**, 24093 (2016).
[23]J. S. Ross, S. Wu, H. Yu, N. J. Ghimire, A. M. Jones, G. Aivazian, J. Yan, D. G. Mandrus, D. Xiao, W. Yao, and X. Xu, Nat. Commun. **4**, 1474 (2013).
[24]B. Radisavljevic, A. Radenovic, J. Brivio, V. Giacometti, and A. Kis, Nat. Nanotechnol. **6**(3), 147 (2011).
[25]A. Sanne, R. Ghosh, A. Rai, H. C. P. Movva, A. Sharma, R. Rao, L. Mathew, and S. K. Banerjee, Appl. Phys. Lett. **106**(6), 062101 (2015).
[26]X. Wang, T.-B. Zhang, W. Yang, H. Zhu, L. Chen, Q.-Q. Sun, and D. W. Zhang, Appl. Phys. Lett. **110**(5), 053110 (2017).
[27]Y. Wang, L. Li, W. Yao, S. Song, J. T. Sun, J. Pan, X. Ren, C. Li, E. Okunishi, Y. Q. Wang, E. Wang, Y. Shao, Y. Y. Zhang, H. T. Yang, E. F. Schwier, H. Iwasawa, K. Shimada, M. Taniguchi, Z. Cheng, S. Zhou, S. Du, S. J. Pennycook, S. T. Pantelides, and H. J. Gao, Nano Lett. **15**(6), 4013 (2015).
[28]Z. Zeng, Z. Yin, X. Huang, H. Li, Q. He, G. Lu, F. Boey, and H. Zhang, Angew. Chem. **50**(47), 11093 (2011).
[29]X. Xi, L. Zhao, Z. Wang, H. Berger, L. Forro, J. Shan, and K. F. Mak, Nat. Nanotechnol. **10**(9), 765 (2015).
[30]K. E. Aretouli, P. Tsipas, D. Tsoutsou, J. Marquez-Velasco, E. Xenogiannopoulou, S. A. Giamini, E. Vassalou, N. Kelaidis, and A. Dimoulas, Appl. Phys. Lett. **106**(14), 143105 (2015).
[31]X. Lin, J. C. Lu, Y. Shao, Y. Y. Zhang, X. Wu, J. B. Pan, L. Gao, S. Y. Zhu, K. Qian, Y. F. Zhang, D. L. Bao, L. F. Li, Y. Q. Wang, Z. L. Liu, J. T. Sun, T. Lei, C. Liu, J. O. Wang, K. Ibrahim, D. N. Leonard, W. Zhou, H. M. Guo, Y. L. Wang, S. X. Du, S. T. Pantelides, and H. J. Gao, Nat. Mater. **16**, 717 (2017).
[32]F. Gong, X. Xu, Z. Li, G. Zhou, and Z. S. Wang, Chem. Commun. **49**(14), 1437 (2013).
[33]M.-Z. Xue and Z.-W. Fu, Electrochem. Commun. **8**(12), 1855 (2006).
[34]I. H. Kwak, H. S. Im, D. M. Jang, Y. W. Kim, K. Park, Y. R. Lim, E. H. Cha, and J. Park, ACS Appl Mater Interfaces **8**(8), 5327 (2016).
[35]35F. Wang, Y. Li, T. A. Shifa, K. Liu, F. Wang, Z. Wang, P. Xu, Q. Wang, and J. He, Angew. Chem. **128**(24), 7033 (2016).
[36]Y. Shen, X. Ren, X. Qi, J. Zhou, G. Xu, Z. Huang, and J. Zhong, J. Mater. Sci.: Mater. Electron. **28**(1), 768 (2016).
[37]N. S. Arul and J. I. Han, Mater. Lett. **181**, 345 (2016).
[38]C. Ataca, H. Şahin, and S. Ciraci, J. Phys. Chem. C **116**(16), 8983 (2012).
[39]J. A. Reyes-Retana, G. G. Naumis, and F. Cervantes-Sodi, J. Phys. Chem. C **118**(6), 3295 (2014).
[40]S. Helveg, J. Vang Lauritsen, E. Lægsgaard, I. Stensgaard, J. Kehlet Nørskov, B. S. Clausen, H. Topsøe, and F. Besenbacher, Phys. Rev. Lett. **84**(5), 951 (2000).
[41]G. Kresse and J. Furthmüller, Phys. Rev. B **54**(16), 11169 (1996).
[42]P. E. Blöchl, Phys. Rev. B **50**(24), 17953 (1994).
[43]G. Kresse and D. Joubert, Phys. Rev. B **59**(3), 1758 (1999).
[44]J. Tersoff and D. R. Hamann, Phys. Rev. Lett. **50**(25), 1998 (1983).
[45]J. Tersoff and D. R. Hamann, Phys. Rev. B **31**(2), 805 (1985).